Vol. 04, No. 3 (2022) 251-262, doi: 10.24874/PES04.03.003

Proceedings on Engineering Sciences

www.pesjournal.net

ECOFRIENDLY LUBRICANT OILS' PERFORMANCE IN LARGE HYDROELECTRIC THRUST BEARINGS

Duriseti V. Srikanth[1]
K. K. Chaturvedi
A. C. Reddy

Received 05.01.2022.
Accepted 31.05.2022.
UDC – 621.822.27-026.9

Keywords:

mesh convergence; hydrodynamic; low toxicity; lubrication

A B S T R A C T

In this paper the modified Reynold's and energy equations of a hydroelectric thrust bearing were solved simultaneously using a scheme of finite differences. Variations in viscosity across the pad film, as well as the hot oil carryover effect, were taken into account. The pad deformation was computed using ANSYS and a linked finite-element technique. A mesh convergence test verified the convergence of the numerical results. The analyzed lubricants were DTE heavy medium oil and a variety of next generation low tox turbine oils. An additional theoretical and established experimental analysis was used to estimate and compare lubricant toxicity. Unlike in previous studies, this study defines the independent factors which control the selection of a lubricant viz. its hydrodynamic efficiency and toxic content.

1. INTRODUCTION

A thrust bearing balances the spinning components and hydraulic load of a big vertical hydropower generator. A THD model of a pivoting pad bearing with radial and circumferential tilt was created (Almquist et al., 2000). The temperature distribution of the pad oil film was taken into account. The viscosity and density were affected by both pressure and temperature. The pressure and runner temperature profiles in the experiments were in good agreement with the theoretical investigations. Low tox turbine oils in the range of grades 6412 to 6414 as described in (Lubricant Engineers, 2015) produced a long-lasting

performance equivalent to the tradititonal turbine oils. They had lower toxic levels than biodegradable turbine oils. They did not need a shortening of lubricant change intervals. They showed excellent demusibilty and were compliant with bearings.

Low tox oils have resulted in a tenfold reduction in eco-toxicity and have been particularly suitable for use in hydroelectric installations. In (Cheng et al., 2015) the efficiency of a water-lubricated thrust bearing was predicted using a finite element approach. Variation and Litz-Galerkin methods were used to derive finite elements from the turbulent Reynold and energy equations. The pressure field obtained was based on the model of finite elements. The pad's load capacity decreased with an increase in temperature. (Saini et al., 2015) investigated the thermophysical characteristics of non-Newtonian surrogate lubricants. A steady state analysis was carried out for the bearings modelled in ANSYS. To generate thermal stress, the temperature changed linearly on the pad's outside surface and non-

[1] Corresponding author: Srikanth Duriseti V.
Email: dvsrikanth@sreenidhi.edu.in

linearly on its inner surface. The study focused on the temperature distribution of the bearings based on the lubricant's dependent thermophysical characteristics. In (Wasilczuk, 2015) the lubricating systems for big tilting pad thrust bearings used in hydropower turbines were examined. The viscous shearing of the lubricant generated a significant quantity of heat, which required forced cooling. Effective oil bath external cooling systems have some advantages compared to internal cooling systems but have become less efficient and simple.

A theoretical analysis of the flow and efficiency parameters of a dimpled thrust bearing was conducted in (Papadopoulos et al., 2013). The incompressible flow numerical solutions of Navier Stokes and energy equations were used to evaluate hydrodynamic efficiency. Realistic boundary conditions were taken into account. This study suggested that proper rectangle dimples textured on parallel thrust bearings resulted in a major increase in load capacity levels. Various pressure profiles with grid independence were analysed in (Najar & Harmain, 2014). The Reynolds equation was solved on the pad surface using FDM techniques to determine the pressure distribution of the oil layer. It was discovered that the grid independence occurred after the 24×24 grid. This study analysed different pressure profiles and confirmed that the refining of the grid could have a major impact on the pressure values. The load-bearing capability of a thrust bearing with an elastic pad was evaluated in (Minculescu, & Cicone, 2005) in order to obtain optimum pad parameters. Thrust bearing analysis software used an FDM solution for flow and thermal equations as well as a FEM solution for pad deformation. Differences in theoretically projected thrust bearing characteristics using two independently developed TEHD models were analysed in (Wodtke et al., 2008). In the two versions, there was a strong agreement on the characteristics of the bearings for the isothermal case. The 2D model projected higher load capacity and loss of power resulting in a difference with experimental values. A strong understanding was reached with the experimental results for the 3D model. Lubricating oils are essential products without which no equipment can operate as discussed in (Bouillon, 2016; Tič and Lovrec, 2019; Lovrec and Tič, 2019). This paper investigated the oxidation resistance and thermal stability properties of lubricants in industrial systems. Laboratory tests for the evaluation of lubricant performance in accordance with OEM, national and international specifications were identified. The analysis of highly refined base oils with very low levels of aromatics and almost no sulphur was conducted in (Gatto et al., 2006). Modern methods for the oxidation of bulk oils using various base materials under varying temperatures, metal catalysts and antioxidants were introduced. The solution to major environmental issues of pollution and degradation of hydrocarbons were discussed in (Das & Chandran, 2011). Bioremediation was the best method for the treatment of this pollution. It was inexpensive and helped to biodegrade and mineralize organic contaminants into, water, carbon dioxide, inorganic chemicals, and cell protein. Biological microorganisms have also been used to convert complex organic pollutants into simpler organic pollutants. Stringent regulations on the use, storage and disposal of lubricants in power plant bearings was discussed in (US Department of the Interior Bureau of Reclamation, 2004). The goal was to use products that were less harmful and more readily biodegradable if they were accidentally released to the environment. A product could be harmful to one organism and not toxic to another. Similarly, a product can easily biodegrade under certain conditions, but not under different conditions. Environmentally safe lubricant oils in use have been regularly checked. The literature review reveals that there are very few studies of the pressure and temperature characteristics of low toxicity lubricant oils in thrust bearings. The purpose of this study is to create quick computational algorithms for evaluating the low tox oil film's hydrodynamic performance, including pad deformation. In addition, a novel independent method for estimating the toxic content of DTE heavy medium and low toxic turbine oils in the range 6412 to 6414 has been developed. Table 1 describes the structure, the working conditions of the bearings and the properties of these turbine oils. Unlike non-newtonian surrogate lubricants, it is noted that there are no major variations in viscosity for DTE heavy medium and low tox lubricants under consideration.

2. OIL FILM SHAPE

The pad film shape as in Figure 1 was defined by the following equation (1).

$$h = A1 - A2x - A3y \tag{1}$$

for $x = r\sin\left(\theta - \theta cp\right)$ and $y = r\cos\left(\theta - \theta_{cp}\right) - r_{cp}$

The following boundary conditions were used to determine the coefficients A1, A2, and A3; the origins of the x and y axes were identified:

- The film thickness h_o at Q was the smallest practicable.
- The thickness of the film along the RS was used and γ' expressed as the thickness ratio of the film in the y-direction.
- The slope between points O and Q was employed as a boundary condition in equation (1) as well.
- The γ' was split into two portions, one was the variable γ and the other that produced a uniform film thickness at the trailing edge γ_o
- Along the trailing edge, the thickness of the film was made invariant.

The equation for the shape of the oil film was presented in its final form by

$$h = h_o\left[1+\left(ar_{cp}\ /\ B\right)\tan\left(\beta-\theta_{cp}\right)\right] - h_o\left(ar/B\right)\sin\left(\theta-\theta_{cp}\right) + h_o\left[\left(a/B\right)\tan\left(\beta-\theta_{cp}\right)-\gamma/L\right]\left[r\cos\left(\theta-\theta_{cp}\right)-r_{cp}\right] \quad (2)$$

Table 1. Geometry of Thrust Bearing

Diameter of the outside	1.275 m			
Diameter of the inside	0.75 m			
Pads in Number	6			
width of the groove	84 mm			
Conditions of Operation				
Load	2.2 MN			
Rotational speed	14.28 rads/sec			
Pot oil temperature	40 º C			
Properties of Oil				
Names of the oils	DTE heavy Medium oil	Low Tox turbine oils		
		6412	6413	6414
ISO grade	68	46	68	100
Viscosity at 40 º C (cSt)	73	45.9	66.3	102.3
Viscosity at 100 º C (cSt)	10.7	6.6	8.64	11.61
ρ (kg/l)	0.861	0.864	0.869	0.871

By dividing both sides with h_o, the following equation (3) for non-dimensional thickness of the oil film was obtained:

$$H = h/h_o = 1+\left(ar_{cp}\ /\ B\right)\tan\left(\beta-\theta_{cp}\right) - \left(a\,r/B\right)\sin\left(\theta-\theta_{cp}\right) + \left[\left(a/B\right)\tan\left(\beta-\theta_{cp}\right)-\gamma/L\right]\left[r\cos\left(\theta-\theta_{cp}\right)-r_{cp}\right] \quad (3)$$

3. MODIFIED REYNOLD'S EQUATION

The following assumptions were used throughout the analysis:

- The oil film was in the steady-state
- The lubricant was newtonian & incompressible.
- Laminar flow was prevalent in the convergent wedge
- Pressure and shear impacts on viscosity were insignificant under the given operating conditions.
- Variations in specific heat and density with pressure were minimal.
- Cavitation was considered if the oil film became divergent owing to crowning or thermo-elastic distortion. The importance of pressure was set to zero everywhere it was negative

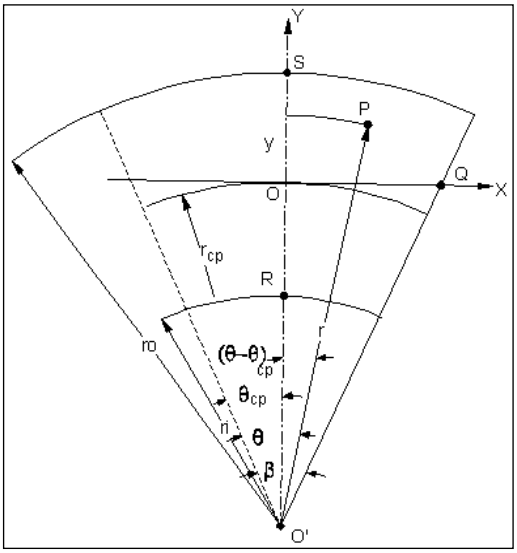

Figure 1. Oil film shape for a flat thrust pad.

The modified Reynolds equation was created by including the lowest order elements of the Navier Stokes equation into the continuity equation, which was then integrated over the film. The Reynolds equation for pressure distribution was used to analyse hydrodynamic thrust bearings. With the increased computing power, numerical models that account for viscosity fluctuations along and across the lubricating layer were created. The temperature of the oil film increased by 15 to 20° C along the sector pad, as in (Ettles, 1991). The temperature of the runner changed by 1°C over its surface, which is substantially less than the temperature of the thrust pad active face. As a result conduction through the pad was not considered.

The pressure field was determined by substituting the viscosity values obtained from the oil film temperature field into the Reynolds' equation. A realistic pressure distribution at the edges was assumed in estimating the load as in (Chaturvedi et al., 1989). Tanaka published a cutting-edge work on thermohydrodynamic design and analysis of bearings in 2000, as reported in (Tanaka, 2000). In equation (4), the Reynolds equation for a sector-shaped thrust segment for an incompressible lubricant under steady-state conditions was reported.

$$\frac{\partial}{\partial r}\left[\frac{rh^3}{\mu}\frac{\partial p}{\partial r}\right]+\frac{1}{r}\frac{\partial}{\partial\theta}\left[\frac{h^3}{\mu}\frac{\partial p}{\partial\theta}\right]=6\omega r\frac{\partial h}{\partial\theta}+12r\frac{\partial h}{\partial t} \quad (4)$$

The following modifications were made to Equation (4) to make it non-dimensional.

$$r = r_o R;\ \theta = \beta\theta \quad \mu = \mu_o \bar{\mu}$$
$$h = h_o H;\ p = \left(r_o^2\, \omega\mu_o / \beta h_o^2\right) P \qquad (5)$$

The Reynolds equation was simplified to a non-dimensional form using the foregoing replacements, as seen in equation (6):

$$2\frac{\partial}{\partial R}\left[\frac{RH^3}{\bar{\mu}}\right]\frac{\partial p}{\partial R} + \frac{2RH^3}{\bar{\mu}}\frac{\partial^2 P}{\partial R^2} + \frac{2}{\beta^2 R}\frac{\partial P}{\partial \bar{\theta}}\frac{\partial}{\partial \theta}\left[\frac{H^3}{\bar{\mu}}\right] + \frac{2}{\beta^2 R}\frac{H^3}{\bar{\mu}}\frac{\partial^2 P}{\partial \bar{\theta}^2} = 12R\frac{\partial H}{\partial \theta} + 24\,R\,\beta\,\frac{\partial H}{\partial t} \qquad (6)$$

When the first derivatives in the preceding equation were changed into second derivative terms, Equation (7) was generated with greater numerical precision.

$$\frac{\partial^2}{\partial R^2}\left[\frac{RH^3 p}{\bar{\mu}}\right] + \frac{RH^3}{\bar{\mu}}\frac{\partial^2 P}{\partial R^2} + \frac{1}{R\beta^2}\frac{H^3}{\bar{\mu}}\frac{\partial^2 P}{\partial \bar{\theta}^2} - \frac{P}{R\beta^2}\frac{\partial^2}{\partial \bar{\theta}^2}\left[\frac{H^3}{\bar{\mu}}\right] - P\frac{\partial^2}{\partial R^2}\left[\frac{RH^3}{\bar{\mu}}\right] + \frac{1}{R\beta^2}\frac{\partial^2}{\partial \bar{\theta}^2}\left[\frac{H^3 P}{\bar{\mu}}\right] = 12R\frac{\partial H}{\partial \theta} + 24R\beta V \qquad (7)$$

4. HEAT ENERGY EQUATION

Thermal impacts from viscous shearing of lubricant layers hinder performance in a variety of ways. Because of the decreased viscosity caused by heat production, the load capacity was reduced. The energy equation governed heat generation and transfer. Pressures and temperatures were calculated using partial differences. The energy equation for a laminar and incompressible flow was given by Equation (8).

$$C_p \rho \left[q_r \frac{\partial T}{\partial r} + q_\theta \frac{1}{r}\frac{\partial T}{\partial \theta}\right] = \dot{E} \qquad (8)$$

Equations (9, 10) calculated radial and circumferential flow, respectively, while equation (11) calculated heat dissipation rate.

$$q_r = -\frac{h^3}{12\mu}\frac{\partial p}{\partial r} \qquad (9)$$

$$q_\theta = \frac{r\omega h}{2} - \frac{h^3}{12\mu}\frac{1}{r}\frac{\partial p}{\partial \theta} \qquad (10)$$

$$\dot{E} = \frac{\mu}{h}(\omega r)^2 + \frac{h^3}{12\mu}\left[\left(\frac{1}{r}\frac{\partial p}{\partial \theta}\right)^2 + \left(\frac{\partial p}{\partial r}\right)^2\right] \qquad (11)$$

The fluctuation of viscosity with temperature was calculated using the Vogelpohl – Cameron equation (12)..

$$\mu = \mu_0 e^{A/(T+95)} \qquad (12)$$

It was incorporated into the iterative process. The known inlet oil temperature was applied to all spots along the oil's entry side. The energy equation in [13] was written in a non-dimensional form.

$$\frac{\partial T}{\partial \theta}\left[nH^2 - \frac{H^4}{12R^2}\left(\frac{L}{R_o}\right)^2\left(\frac{\partial P}{\partial \theta}\right)\right] - \frac{H^4}{12}\left(\frac{L}{R_o}\right)^2\left(\frac{\partial P}{\partial R}\right)\left(\frac{\partial T}{\partial R}\right) = 4n^2R^2 + \left(\frac{L}{R_o}\right)^4\frac{H^4}{12}\left[\left(\frac{\partial P}{\partial R}\right)^2 + \frac{1}{R^2}\left(\frac{\partial P}{\partial \theta}\right)^2\right] \qquad (13)$$

5. HOT OIL CARRYOVER

The hot runner in the inter-pad gap heated the lubricant as it entered the wedge at the inlet edge. This lubricant also included some oil from the previous pad and some oil from the bath to compensate for the oil lost owing to side leakage. As a result, the actual intake temperature in the oil film exceeded the bulk oil temperature. This effect was researched and analysed experimentally for numerous thrust bearing types in (Ettles, 1969). The impact of hot oil carry over was shown as

$$T_{out} = T_{sup} + \Delta T\left(\frac{2-k}{2-2k}\right) \qquad (14)$$

where the hot oil carry over coefficicent *k* was

$$k = \frac{T_{in} - T_{supp}}{T_{run} - T_{supp}} \qquad (15)$$

assumed in this study to be = 0.83. Based on the trials, this coefficient was determined by the ratio of oil film intake gap to oil film outflow gap.

$$T_{in} = T_{out} - \Delta T \qquad (16)$$

Once the temperature of the housing bulk oil and temperature increase are known, the runner temperature and output temperature may be computed using eq.(16).

6. PAD DEFORMATION

The pad linked thermo-structural deformation was determined using a finite element analysis with ANSYS. Equation (17) gave the thermal structural deformation equation.

$$[K]\{U\} = \{R\} + \{r\} \qquad (17)$$

[K] represented the structural matrix for stiffness. {U}, {R} and {r} represented the nodal displacement, applied

temperature, and applied pressure loading vectors respectively. The hexahedral solid 226 elements were used to mesh the pad thermo-structural deformation model. Each element would have up to twenty nodes and each node up to five degrees of freedom. Only elastic structural capabilities were available, including considerable deflection and stress stiffening. The restored nodal film thickness was equal to the sum of the original film thickness and the related nodal distortion.

7. MESH INDEPENDENCE TEST

The mesh independence test, as described in (Srikanth D.V., Chaturvedi K.K., Reddy A.C, 2014), was carried out in the following manner. The preliminary simulation was done using an 11 × 11 nodal mesh, and the Rcp, θcp and load values were determined to be 1.0571m, 0.2625 radians and 2.037e^6 N respectively. The mesh was refined to a 10 × 10 nodal matrix because these values had not converged to the appropriate ones. In this situation, the values for Rcp, θcp, and load were 1.0565m, 0.2603 radians, and 2.0957e^6 N, respectively. These readings had not converged to the recommended values, either. This demonstrated that the solution varied as a result of the mesh resolution, implying that it was not yet independent of the mesh. The mesh was improved further to a 9 × 9 nodal matrix, yielding Rcp, θcp and load values of 1.0557 m, 0.2575 radians and 2.1663e^6 N. For the 4.5 MPa maximum nodal pressure distribution, these converged to within 1% of the previously stipulated values. The mesh-independent solution was reached by selecting the lowest size while decreasing simulation duration. In addition, the test ensured that it was not the mesh resolution that was instrumental in the results but the physics and boundary conditions.

8. HYDRODYNAMIC COMPUTATIONAL METHOD:

The mesh independence solution called for a grid of 81 nodes, as illustrated in Figure 2, for the FDM discretization of the film. In order to solve the Reynolds' equation, the central difference form of the truncated Taylor series expansion was utilized.

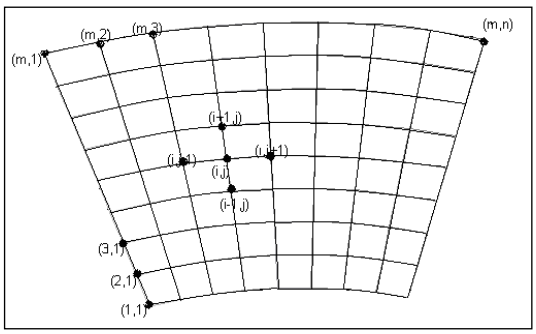

Figure 2. Pad discretization in Reynolds' equation

To assess the derivatives, the functional values of neighboring nodes on either side were necessary. By expressing the Reynolds equation in finite difference form, as shown in Eq. (18), a set of linear algebraic equations was generated.

$$P_{i+1,j}\left[\frac{R_{i,j}H_{i,j}^3}{\Delta R^2\overline{\mu}_{i,j}}+\frac{R_{i+1,j}H_{i+1,j}^3}{\overline{\mu}_{i+1,j}\Delta R^2}\right]$$
$$+P_{i-1,j}\left[\frac{R_{i,j}H_{i,j}^3}{\Delta R^2\overline{\mu}_{i,j}}+\frac{R_{i-1,j}H_{i-1,j}^3}{\overline{\mu}_{i-1,j}\Delta R^2}\right]$$
$$+P_{i,j+1}\left[\frac{H_{i,j}^3}{R_{i,j}\overline{\mu}_{i,j}\beta^2\Delta\overline{\theta}^2}+\frac{H_{i,j+1}^3}{R_{i,j}\overline{\mu}_{i,j+1}\beta^2\Delta\overline{\theta}^2}\right]$$
$$+P_{i,j-1}\left[\frac{H_{i,j}^3}{R_{i,j}\overline{\mu}_{i,j}\beta^2\Delta\overline{\theta}^2}+\frac{H_{i,j-1}^3}{R_{i,j}\overline{\mu}_{i,j-1}\beta^2\Delta\overline{\theta}^2}\right]$$
$$+P_{i,j}\left[-2\frac{R_{i,j}}{\Delta R^2}\frac{H_{i,j}^3}{\overline{\mu}_{i,j}}-\frac{R_{i+1,j}}{\overline{\mu}_{i+1,j}}\frac{H_{i+1,j}^3}{\Delta R^2}-\frac{R_{i-1,j}}{\overline{\mu}_{i-1,j}}\frac{H_{i-1,j}^3}{\Delta R^2}\right.$$
$$\left.-2\frac{H_{i,j}^3}{R_{i,j}\overline{\mu}_{i,j}\beta^2\Delta\overline{\theta}^2}-\frac{H_{i,j+1}^3}{R_{i,j}\overline{\mu}_{i,j+1}\beta^2\Delta\overline{\theta}^2}-\frac{H_{i,j-1}^3}{R_{i,j}\overline{\mu}_{i,j-1}\beta^2\Delta\overline{\theta}^2}\right]$$
$$=\frac{6R_{i,j}}{\Delta\theta}\left[H_{i.j+1}-H_{i,j-1}\right]+12R_{i,j}\,\beta V \tag{18}$$

The aforementioned equation was written for each node, yielding a set of simultaneous linear algebraic equations as a result.

$$A1_k\,P_{k+1}+A2_k\,P_{k-1}+A3_k\,P_{k+m}+A4_k\,P_{,k-m}+A5_k\,P_k=A6_k \tag{19}$$

Eq. (19) was transformed into matrix form with the following substitutions:

$$C_{k,k+1}=A1_k/A5_k$$
$$C_{k,k-l}=A2_k/A5_k$$
$$C_{k,k+m}=A3_k/A5_k$$
$$C_{k,k-m}=A4_k/A5_k$$
$$C_{k,k}=1$$
$$AC_k=A6_k/A5_k \tag{20}$$

In the matrix form, the equations (20) were written as:

$$[C]_{mn,mn}[P]_{mn,1}=[AC]_{mn,1} \tag{21}$$

Eq. (21) was solved by matrix inversion and multiplication with available subroutines to yield the nodal non-dimensional pressure. Load capacity and centre of pressure location were obtained by integrating these pressures.

The Reynolds equation's boundary conditions were addressed as

$$P = 0 \text{ at } r = r_i, r = r_o, \theta = 0, \theta = \beta \qquad (22)$$

In the non-dimensional form, these conditions were expressed for all nodal values of k lying on the boundary as

$$P_{i,j} = P_{m,j} = P_{i,l} = P_{i,n} = 0 \qquad (23)$$

These equations were put in a form similar to (19) and were incorporated in the matrices C and AC. The elements of the matrices were assigned the following values for all nodes on the border.

$$C_{kl} \text{ for } {}_{k \neq l} = 0; C_{k,k} = 1 \text{ and } AC_k = 0 \qquad (24)$$

The energy equation was also solved using finite differences. As the energy eq. (8) depends on the pressure gradient it was solved simultaneously with the Reynolds equation using the same grid.

The energy equation, which included the components $\frac{\partial T}{\partial r}$ and $\frac{\partial T}{\partial \theta}$, was written in finite differences to represent the local heat dissipation and $\frac{\partial T}{\partial r}$ in terms of $\frac{\partial T}{\partial \theta}$. The first order of the equation shows that it was solved using the propagation technique. The temperature was provided along the whole leading edge, such that the starting values of $\frac{\partial T}{\partial r}$ were also known. The following equations presented $\frac{\partial T}{\partial r}$ with temperature variation between neighbouring nodes in the circumferential and radial directions

$$\frac{\partial T}{\partial r} = \frac{1}{2dr}\left[4T_{k+1} - 3T_k - T_{k+2}\right] \text{ in the forward difference form} \qquad (25)$$

$$\frac{\partial T}{\partial r} = \frac{1}{2dr}\left[T_{k+1} - T_{k-1}\right] \text{ in the central difference form} \qquad (26)$$

$$\frac{\partial T}{\partial r} = \frac{1}{2dr}\left[T_{k-2} + 3T_k - 4T_{k-2}\right] \text{ in the backward difference form} \qquad (27)$$

$\frac{\partial P}{\partial \theta}$ and $\frac{\partial P}{\partial R}$ were stated in the same way as $\frac{\partial T}{\partial r}$ with fluctuations in pressure As a result, the temperature of the downstream node was calculated as follows

$$\frac{\partial T}{r\partial \theta} = \frac{\left[\frac{\dot{E}}{\rho C p} - \frac{h^3}{12\mu}\frac{\partial p}{\partial r}\frac{\partial T}{\partial r}\right]}{\left[\frac{r\omega h}{2} - \frac{h^3}{12\mu}\frac{1}{r}\frac{\partial p}{\partial \theta}\right]} \qquad (28)$$

where, $\frac{\partial T}{r\partial \theta} = \frac{1}{2r_k \Delta\theta}\left[T_{k+1} - T_{k-1}\right]$ (29)

Using this approach, the temperature distribution was determined in a single sweep while accounting for the hot oil carry over effect. When the Vogelpohl-Cameron equation was included in the energy equation, the temperature fluctuated throughout the flow of oil. The Reynolds equation was solved using the original uniform temperature and viscosity distribution data. q_r & q_θ were calculated using equations (9) & (10). Eq.(8) was solved for $T(r,\theta)$ and therefore μ(T). Using the new distribution of viscosity, the Reynolds' equation was resolved for pressure. This iterative scheme converged quickly. ANSYS was used to calculate the coupled thermo-structural deformation of the pad using a finite element approach. The thrust pad geometry corresponded to the values in Table 1. Table 2 shows the input thermal and structural parameters of the pad material.

The initial phase in the investigation was to create a solid model and mesh it. To the greatest degree feasible, the problem symmetry was employed. This reduced the physical dimension and allowed for the adoption of the lowest mesh-size. The model was produced in the axi-coordinate system by connecting critical points, forming regions, and working around the axis. After that, the model was meshed using Solid 226 components and simulated for a load step. The nodal values of the elements of the bottom surface were identical to the corresponding values of the lubrication problem. The analysis was therefore coupled. There were 8 radial, 8 circumferential, and 8 longitudinal thickness elements in the linked thermo-structural deformation elemental plot of the pad, for a total of 512 hexahedral elements.

The pressure and load were applied to the bottom surface area A2 using the axi-symmetric boundary condition.

The convective heat transmission from Figure 3's regions A1, A3, A4, and A6 was studied. The bulk oil temperature was 40°C, and the convection film coefficient was 4e6.

Table 2. Pad Mechanical Properties

Mechanical Properties of Pad	
The Young's modulus (GPa)	195
The Poisson's ratio	0.29
The degree of density (Kg/m$^{3)}$	7850
Thermal Properties of a Pad	
Thermodynamic expansion/ °C	12.2e^{-6}
Thermal conductivity (W/m-K at 10°C)	42.6
Specific heat (J/kg-K)	473
Inner surface heat transfer coefficient	6.015e^{-4}
Outer surface heat transfer coefficient	30e^{-6}

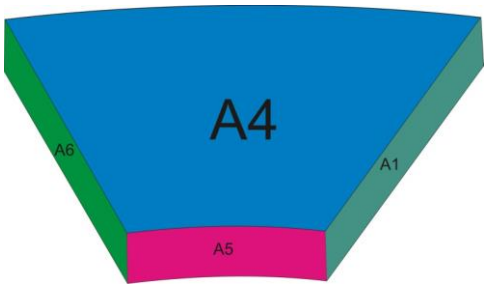

Figure. 3. Load-bearing and heat-transfer zones

The heat flux values derived from the energy equation solution were the same for the bottom pad's elemental surface nodes.

The heat transmission from the pad via radiation was ignored.

The load step was used to see the results of the deformation function. Plot result, counter plot, nodal solution, and displacement vector functions were used.

The computed thermoelastic deformation was used to modify the oil film, yielding new- pressure and temperature profiles that were then imported back into the ANSYS model.

9. HYDRODYNAMIC RESULTS AND DISCUSSIONS:

The pad deformed to a maximum of 0.896e-3 m at the bottom and outside circumferential edge in the coupled field analysis, as shown in Figure 4 for the 40mm thick pad. The pad deformations were of the same order of magnitude as the oil film thickness, which was in both cases to the order of 6μm. Figure 5 depicts the pressure distribution for a standard turbine oil's film. Figure 6 shows the corresponding pressure distributions for the low toxic 6414 grade oil. The pressure applied to the pad surface's leading edge was minimal. The pressure production was substantial in the area of the pad surface's trailing edge. The highest peak pressure was slanted to the trailing edge. The peak value of the pressure was reached when film thickness was minimum and counteracted the sliding surface external load. The temperature distributions for the above tested oils were shown in Figure 7 and Figure 8 and they were characteristic of the viscosity values. The predominance of maximum temperature was signified by the border region of minimal film thickness and maximum rotation speed. The highest film temperature rise was seen at the trailing edge corner at the outer radius. The highest temperature was found at the intersection of the trailing edge and the outer radius. When comparing the left and right halves of the pad, the temperature change was smaller along the left side. The study revealed that the 6414-grade lubricant had the greatest maximum pressure and temperature, while the 6412 grade lubricant had the lowest. The oils were able to adapt effectively to boundary lubrication conditions during start up and shutdown.

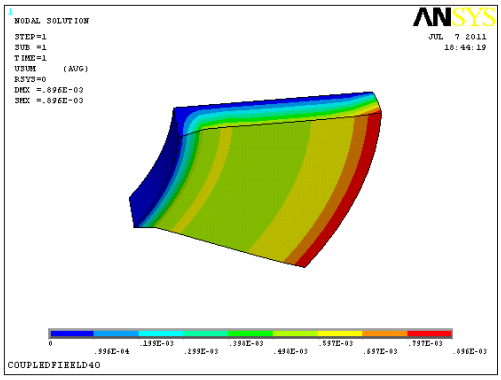

Figure 4. Deformation distribution of a coupled field.

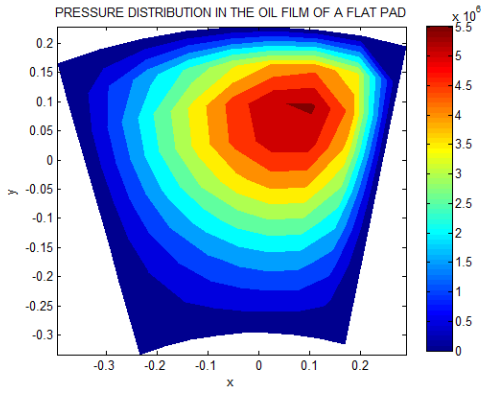

Figure 5. The traditional turbine oil film's pressure distribution

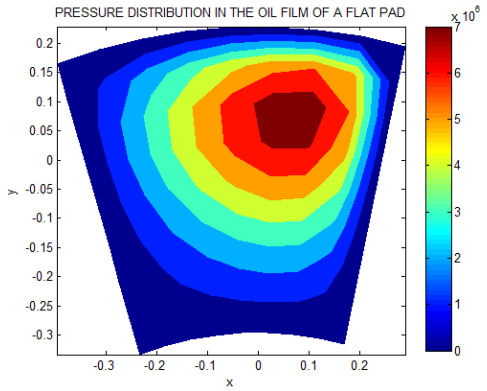

Figure 6. Pressure distribution in a low toxicity oil film of grade 6414

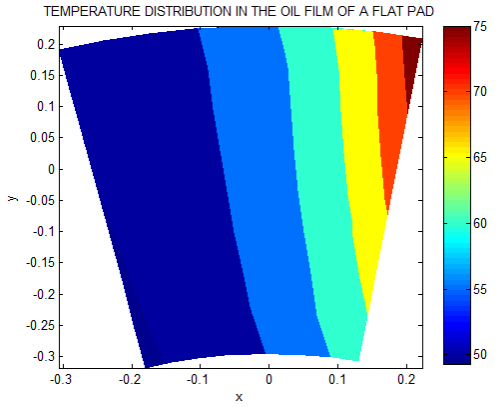

Figure 7. The traditional turbine oil film's temperature distribution

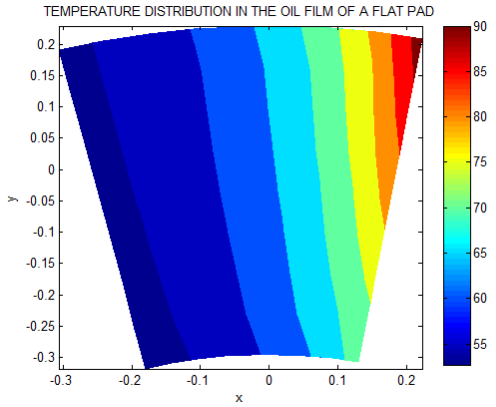

Figure 8. Temperature distribution in the low toxicity oil film 6414 grade-

9.1. Validation

The accuracy of the author's theoretical predictions using data in Table 1 is compared with experimental data results of (Yuan et al., 2001) and (Zhong & Zhang, 2011). As in Figure 9. the experimental pressures were lower than those of theory. The relatively considerable disparities between the experimental data and the author's theoretical data were due to flaws in the theoretical modelling. Because predicted pressures were somewhat greater than observed pressures, the software programme overestimated pressure in areas where no measurements were recorded. The difference in temperatures as in Figure 10. was on account of variation in input temperatures and viscosity. The differences in pressure and temperature were large as speeds and oil viscosities were higher for Yuans's data as with larger bearing diameter and load for Zhong De's data. Although not perfect, agreement with theoretical and practical results provided substantial evidence for the software package's value in forecasting large thrust bearing performance.

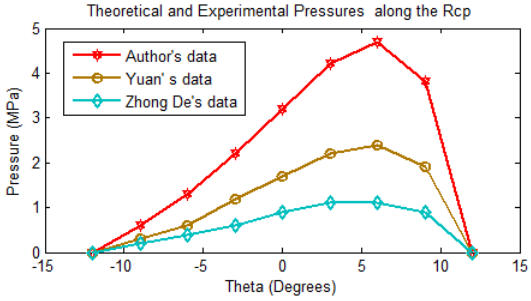

Figure 9. Pressures along the R cp, both theoretical and experimental

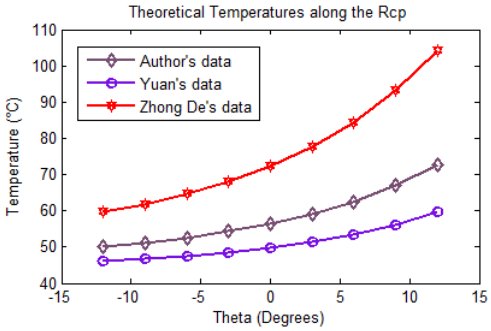

Figure 10. Temperatures along the R cp, both theoretical and experimental

10. LUBRICANT OIL TOXICITY:

A Toxicological research was conducted to quantify the toxicity of turbine oils, namely DTE heavy medium oil, low tox, and used turbine oils, in the terrestrial environment over a predetermined biodegradation time. Toxicity levels were determined during the biodegradation period using Eruca Sativa (arugula seeds) and Eisenia Andrei (earthworms), as in (Tamada et al., 2012). This study provided an indirect evaluation of microbial metabolism efficiency in pollutants by evaluating the biodegradation process.

Abbots' formula viz. $I\% = \frac{(C-T)\times 100}{C}$ was used where I % denotes the percentage of inhibition, C- represents the number of germinated seeds in the negative control, and T refers to the number of germinated seeds in the sample treated

a. The oil was deemed harmful when germination inhibition of seeds was greater than 40%, according to the toxicological examination.
b. When germination inhibition was between 10% and 40% there was onset of toxicity
c. Not harmful when inhibition present was 10%.

In Figure 11, utilizing E. Sativa seeds, the oils had an initial high toxicity of more than 75% in all cases. The toxicity of the DTE heavy medium oil increased for 60 days and decreased thereafter. The toxicity of the new LE low tox oil dropped after the iniitial adaption time, but the toxicity of the used turbine oil remained high throughout the duration.

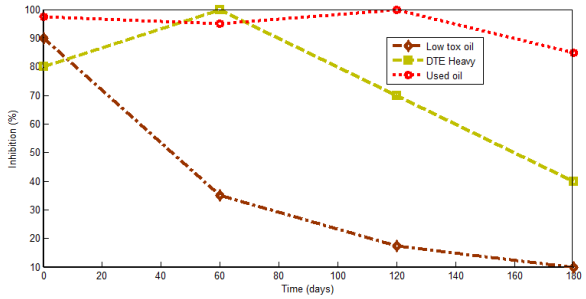

Figure 11. Toxicity of turbine oils (E. sativa) after 0, 60, 120, and 180 days of biodegradation

The results in Figure 12 for E. Andrei showed that the toxicity of the LE low tox and DTE heavy medium oils had diminished in the 180-day period.The first showed no toxicity at the conclusion of the session, but the DTE heavy oil showed 5%. The toxicity of the utilized oil did not diminish. Because of the high working pressure and temperature, the utilized oil molecules were more decomposed. This was explained by the presence of contaminants which did not degrade in the given period.

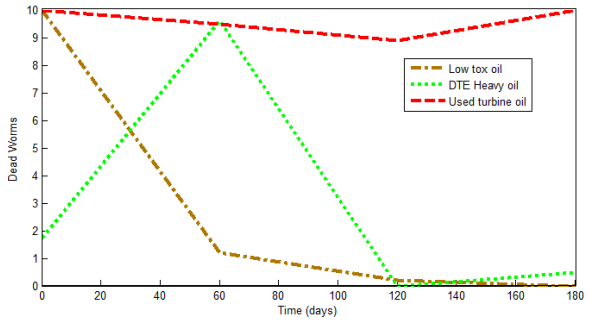

Figure 12. Toxicity of turbine oils (E. Andrei) after 0, 60, 120, and 180 days of biodegradation

The above results were compared and validated with the Microtox Luminiscent bacteria bioassay test results in (Lubricant Engineers, 2015). The effective concentration was determined in milligrams of oil per litre of water, and the EC50 values represented that. It displayed the effective concentration of the substance being tested as well as the amount required to lower bacterial luminescence metabolic activity by 50%. The EC values applied to oils that were not water soluble. The higher EC values indicated lower toxicity and vice versa. The EC value of the low tox 6413 grade oil tested was 112580 mg/l and that of DTE heavy oil was 48230 mg/l. In 28 days the low tox oils were biodegradable by 55%.

11. CONCLUSIONS

The finite difference approach was utilised in this work to solve the Reynolds and Energy equations of the large oil lubricated tilting pad thrust bearing. Low tox oils in the range of 6412-6414 were analyzed and the pressure and temperature profiles plotted. The toxicity values of DTE heavy medium, low tox and used turbine oils were estimated over the bio-degradation period range of 0 to 180 days. According to the E. Andrei results biodegradation was effective for the LE low tox and DTE Heavy medium oils. The LE low tox oil had its toxicity dramatically reduced in only 50 days. The application of low tox turbine oils was justified as they possessed excellent demulsibilty and were compatible with mechanical seals. They had minimum adverse impact on the environment. To the best of the knowledge of the authors this study was unique in highlighting the importance of hydrodynamic performance and toxicity in the selection of a lubricant.

12. ABBREVIATIONS

a : the form of the oil film parameter, $(h_o- h_i)/ h_o$
h_o : trailing edge oil film thickness, m
h_i : leading edge oil film thickness, m
i : radial node index
j : circumferential node index
k : composite node index
m : number of radial nodes on the grid
n : number of circumferential nodes on the grid
p : oil film pressure, Pa
r : coordinate in radial direction, m
r_o : bearing's outer radius, m.
B : circumferential length of the thrust pad, m
C_P : pressure centre
D_i : thrust bearing's inner diameter,m
D_o : thrust bearing's outer diameter, m
H : oil film's non-dimensional thickness, h/ho
L : thrust pad's radial length, m
N : runner's angular speed, rpm
P : pressure that is not dimensional, $\frac{ph^2}{\mu U}$
P :Reynolds' equation's pressure matrix
R :radius that is not dimensional, r/r_o
R_{cp} : pressure center's radial coordinate, m
T :Temperature of lubricant, ˚C
U, V :Parallel and normal velocity to surface, m/s
W :bearing load, N
X : pressure centre x-coordinate
Z :Pad's count
β : thrust pad's angular extent.
γ :ratio of film thickness
μ :oil viscosity, Pa.s
$\bar{\mu}$:viscosity that is non dimensional
θ :angle relative to the leading edge, radian
θ_{cp} : pressure centre angular position, radian.
ρ :oil density, kg/m3
ω :runner angular velocity, radian /s
Δ r :radial grid division , m
Δ v :grid element volume, m^3
Δ θ :grid angular division, radian.
Δx : Displacement differential,

References:

Almquist T., Glavatskikh S. B. & Larsson R. (2000). THD Analysis of Tilting Pad Thrust Bearings-Comparison Between Theory and Experiments. *Journal of Tribology*, *122*(2), 412-417.

Bouillon V. (2016). Overview of oxidation laboratory tests on industrial lubricants. In*: Euskalduna conference centre.* Bulbao, Spain, 7th -8th June.

Chaturvedi, K. K., Athre, K., Nath Y., & Biswas, S. (1989). Refinement in Estimation of Load Capacity and Temperature Distribution of Pad Bearing, *Proceedings of Eurotrib-89*, 5th International Conference on Tribology, Helisinki, Finland.

Cheng, D., Yao, Z., & Xue, Y. (2015). Study on the Water Lubricated Large-scale Tilting Pad Thrust Bearing by Finite Element Method. *Proceedings of the World Congress on Engineering and Computer Science*, October 21st -23rd, San Francisco, USA.

Das, N., & Chandran, P. (2011). Microbial Degradation of petroleum Hydrocarbon Contaminants: An overview. *Biotechnology Research International*, *2011*, 1-13.

Ettles C. M. M. (1991). Some Factors Affecting the design of Spring Supported Thrust Bearings in Hydroelectric Generators. *Journal of Tribology- Transactions of the ASME, 113*, 626-632.

Ettles, C. M. M. (1970). Hot Oil Carry-Over in Thrust Bearings. *Proceedings of the Institution of Mechnical Engineers,* 184, 12: 75

Gatto V., Moehle W. and Cobb T. (2006). Oxidation fundamentals and its application to Turbine oil testing. *Journal of ASTM International*, *3*(4), 1-20.

Lovrec, D., & Tič, V. (2019). Excellent lubricating properties of ionic liquid – myth or truth. *Proceedings on Engineering Sciences*, *1*(1), 555–562. https://doi.org/10.24874/PES01.01.073

Lubricant Engineers (2015). *Product specification Handbook*, Asset Reliability solutions, pp.1-2.

Minculescu, A., & Cicone T. (2005). Parametric Analysis of a Hydrodynamic Thrust Bearing with Elastic Slider. *The Annals of University "Dunărea De Jos "of Galaţi Fascicle VIII*, 101-106.

Najar F. A., & Harmain G. A. (2014). Numerical Investigation of Pressure Profile in Hydrodynamic Lubrication Thrust Bearing. *International Scholarly Research Notices*, pp 1-8.

Papadopoulos, C. I., Kaiktsis, L., & Fillon, M. (2013). CFD Thermohydrodynamic analysis of 3-D sector-pad Thrust bearings with Rectangular Dimples. *Proceedings of ASME Turbo Expo 2013*, San Antonio, USA, June 3rd -7th , Texas:ASME.

Saini, V., Raja Sekhar, D., & Kumar, A. (2015). Thermal Analysis on Thrust Pad Bearing with Non-Newtonian Lubricant. *Internationa*l *Journal of Engineering Research & Technology*, *4*(3), 1140-1146.

Srikanth, D. V., Chaturvedi, K. K., Reddy, A. C. (2014). Mesh Independence and Convergence Test in the Oil Film Characteristics of a Tilting Pad Thrust Bearing. *International Conference on Advanced Materials and Manufacturing Technologies*, Hyderabad, India, December 18th -20th , 1: 205-209.

Tamada I. S., Paulo R. L., Renato N. M., & Ederio, D. B. (2012). Biodegradation and toxicological evaluation of lubricant oils, *Brazilian archives of biology and technology, 55*(6).

Tanaka, M. (2000). Recent Thermohydrodynamic analyses and designs of Thick-film Bearings. *Journal of Engineering Tribology, 214*(1), 107-122.

Tič, V., & Lovrec, D. (2019). On-line condition monitoring of hydraulic oils – understanding the results. *Proceedings on Engineering Sciences*, *1*(1), 636–640. https://doi.org/10.24874/PES01.01.083

US Department of the Interior Bureau of Reclamation, (2004). *Lubrication of Powerplant Equipment, Facilities, Instructions, Standards, and Techniques,* Denver,Volume 2-4, pp. 23-27.

Wasilczuk, M. (2015). Friction and Lubrication of Large Tilting-Pad Thrust Bearings. *Lubricants, 3*, 164-180.

Wodtke, M., Fillon, M., & Wasilczuk, M. (2008). Predicting performance of thrust bearings with use of contemporary models. *7th EDF/LMS Workshop on Operational Limits of Bearings: Improving of Performance through Modelling and Experimentation at Futuroscope,* October, Volume: pp. 1-8.

Yuan, J. H., Paulo R. L., Renato N. M., & Ederio D. B. (2001). Spring supported Thrust Bearings Used in Hydro-Electric Generators: Comparison of experimental data with numerical predictions. *Tribology Transactions, 44*(1), 27-34.

Zhong-De, W., & Zhang, H. (2011). Performance Analysis of Thrust Bearing for Three Gorges Generator. *Large Electric Machine and Hydraulic Turbine*, 2(3).

Duriseti V. Srikanth
Sreenidhi Institute of Science and Technology,
Hyderabad Telangana, India
dvsrikanth@sreenidhi.edu.in

K. K. Chaturvedi
Retd. Senior DGM.
BHEL(R&D)
Kalpataru, Adhoiwala, India
ckaushal49@gmail.com

A. C. Reddy
Professor of Mechanical Engineering
JNTUH, College of Engineering
Kukatpally, Telangana, India
dr_acreddy@yahoo.com